Quantification of local fiber distribution for optimization of tape laying techniques

T. Guglhoer[a*], F. Manger[b], M. G. R. Sause[a]

[a]*Institute of Physics, Experimental Physics II, University of Augsburg, 86153 Augsburg, Germany*
[b]*Fraunhofer Institute of Chemical Technology, Project Group Functional Lightweight Design, Fraunhofer Institute, 86159 Augsburg, Germany*
**thomas.guglhoer@physik.uni-augsburg.de*

Keywords: Fiber volume fraction, image processing, fiber distribution.

Abstract
An image processing routine is proposed to quantify distribution of fibers on different length scales in unidirectional fiber reinforced composites. For this purpose the proposed image analysis is validated utilizing artificial images and subsequently demonstrated in application to micrographs of carbon fiber reinforced Polyamid-6 tapes and corresponding laminates fabricated by automated tape laying. We use 2D-mean filters with varying diameter to systematically reduce the image information to the characteristic length scale and to obtain the respective local fiber volume fraction. The results indicate a correlation between the microstructure of the tapes and the distribution of fibers within the corresponding laminate.

1. Introduction

The spatial distribution of fibers in fiber reinforced polymers influences the mechanical performance of the composites. In particular, damage development is linked to local stress concentration which arises from non-uniform arrangements [1,2,3,4]. These are not only induced during mechanical loading but also during the processing of the composites due to different thermal expansion coefficients of the constituents [2,5] or shrinkage of the polymer upon curing [1]. In case of thermoplastic matrix systems the compaction of the textile structure leads to additional stress components in the out-of-plane direction, which correlate strongly with the local fiber distribution [6,7].

Fiber distribution is commonly characterized by image analysis applied to micrographs. For this purpose, area segmentation techniques like Voronoi tessellation [8,9] and Dirichlet tessellation [10] are applied and fiber distribution is given in terms of areal fractions. In contrast, position based methods like the nearest neighbor approach [11,12] or description of inter-fiber spacing [1,2,13] provide the fiber distribution in terms of length distances and are used successfully as well. In common, these methods are based on single fiber detection via threshold methods or pattern recognition techniques.

However, single fiber detection is only applicable to high contrast images and therefore is limited to high resolution images. To avoid this limitation, we propose a method which can be applied to quantify fiber distribution directly based on the grayscale distribution. For this purpose, the average grayscale is determined locally by mean filters of various diameters and

directly correlated with fiber volume fraction. With this method, local fiber volume fractions on different length scales can be determined and evaluated by a statistical approach. In the following, the image processing method is described in detail and, subsequently, applied to characterize fiber distribution of artificial images to validate the method. Furthermore the method is applied to micrographs taken from fiber reinforced polyamide-6 tapes and corresponding laminates. The results indicate that the fiber distribution of tapes and corresponding laminates can be correlated.

2. Material and method

2.1. Material

Two different types of carbon fiber reinforced Polyamid-6 tapes, denoted as tape T1 and T2 were investigated. Both tapes were sliced into 50 mm width. The thickness was determined by optical inspection at 50 positions; we found values of 140±3 µm for tape T1 and 162±14 µm for tape T2, respectively. It is worth noting that tape T1 was produced using 12k and tape T2 using 50k rovings. The fiber diameter in both tapes is approximately 7 µm.

Both tapes were processed via automated tape laying using a Fiber Forge Relay2000 system. The obtained unidirectional laminates are denoted as P1 and P2 corresponding to the tapes T1 and T2 used. For consolidation the laminates were heated on a contact heater to 265°C and subsequently pressed at 50 bar. The laminates were approximately 2 mm thick and 400 x 400 mm wide. The tapes were dried for 6 h at 80°C prior to consolidation.

2.2. Micrographs

For preparation of micrographs, we cut the tapes and laminates into samples of 30 mm length and subsequently embed them into epoxy resin. The whole width of the tapes is inspected. In case of the laminates 6 samples were taken equally distributed along one cross section of the laminate perpendicular to the fiber direction. The curing temperature of the epoxy resin is below 50°C and therefore below the glass transition temperature of Polyamide-6. Grinding was performed using silicon carbide paper. A composite disc with abrasives of 9 µm, 6 µm, 3 µm, 1 µm and subsequently ¼ µm diameter was used for polishing. Using a Keyence VHX-2000 digital microscope, 30 images were taken of the tapes using a 500x objective and 15 images of the laminates using a 100x magnification factor. To enhance the contrast "reflection reduction mode" was used.

2.3. Image Processing

The image processing method to determine local fiber volume fractions on various length scales from micrographs is described in the following. Figure 1 shows the processing steps, which includes sample detection (a-e), fiber-matrix separation (f), and extraction of local fiber volume fractions (g-h).

First, the edges of the sample are detected. Therefore, a local threshold filter converts the grayscale image (a) into binary format whereby areas of high and low contrast are separated (b). A median filter is applied to locally average the binary grayscale values (c). Subsequently, we fit the grayscale values of each row using a rectangular function (d). The positions of the steps coincide with the edges of the specimen and define the region of interest (e).

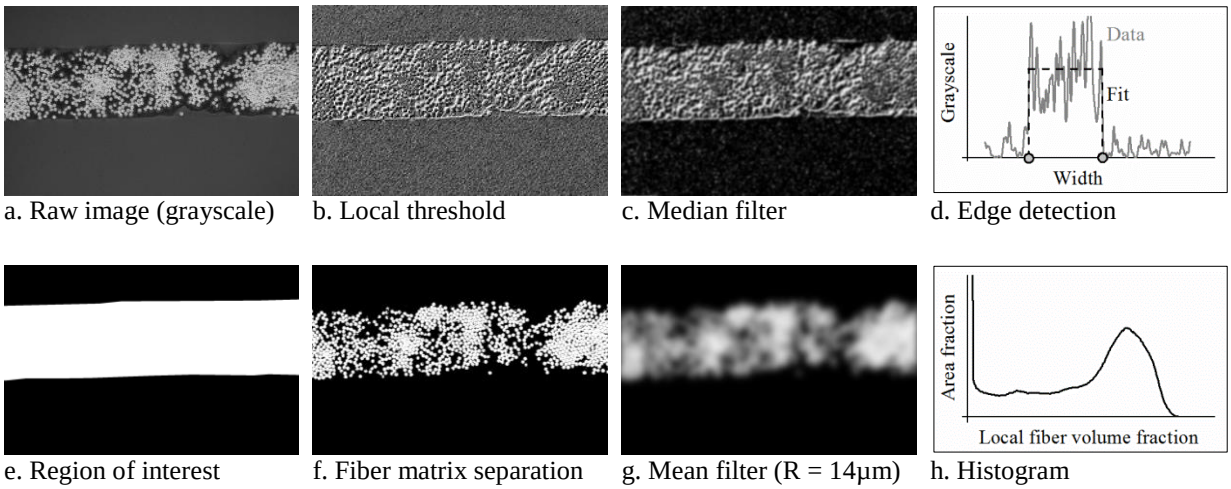

a. Raw image (grayscale) b. Local threshold c. Median filter d. Edge detection

e. Region of interest f. Fiber matrix separation g. Mean filter (R = 14µm) h. Histogram

Figure 1. Steps of image processing

In case of high resolution images, fiber and matrix are separated within the region of interest using a threshold filter according to Otsu [14] (f). From the binary image we obtain locally averaged gray scale values using a mean filter (g). The specific diameter of the mean filter is obviously equal to the length scale of observation. To avoid influences arising from the edge of the specimen the region of interest is reduced at each edge by the size of the radius of the mean filter. Finally the gray value histogram of the reduced region of interest is extracted and the gray scale values are converted into fiber volume fractions using a linear interpolation scale between 0% and 100%. Furthermore, the relative number of pixels for each gray value is equal to the area fraction of the respective fiber volume fraction (h).

The steps mentioned before are performed using the mean filter diameter as additional parameter to obtain local fiber volume fractions on different length scales. The results are visualized in waterfall diagrams. Therefore, two-dimensional representation of area fraction and local fiber volume fraction is extended to a three-dimensional representation using the length scale of observation as third axis. Reasonable choice for the minimum length scale to investigate is the fiber diameter, which is 7 µm, here. Obviously, the maximum length scale is limited by the dimensions of the sample. To obtain information from at least two third of the specimen area and considering the image reduction method we limit the maximum length scale to one third of the smallest sample dimension.

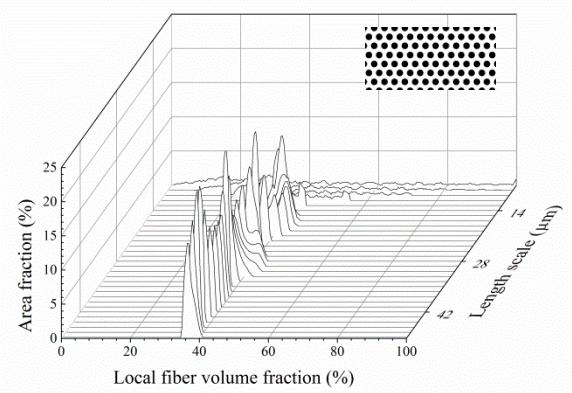

Figure 2. Area fraction of local fiber volume fractions in dependence of the observed length scale for uniform distributed fibers and a total fiber volume fraction of 37%

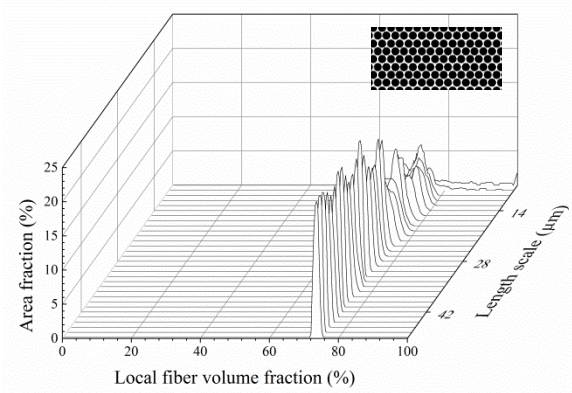

Figure 3. Area fraction of local fiber volume fractions in dependence of the observed length scale for uniform distributed fibers and a total fiber volume fraction of 73%

3. Results

In the following, we apply the image processing method to a set of artificial images with uniform distributions but different fiber volume fractions. In the same section we use artificial images with non-uniform distributions to discuss more realistic structures. Furthermore, the image processing method is then applied to carbon fiber reinforced Polyamid-6 tapes and laminates produced from them.

3.1 Artificial images

The image processing method is validated utilizing artificial images of uniform distributed fibers. Therefore, a set of images showing fibers of 7 µm diameter arranged in a hexagonal array and various total fiber volume fractions was created. Artificial images containing total fiber volume fraction of 37% and 73% and corresponding results are shown in Figure 2 and Figure 3, respectively. Both figures indicate a peak in the area fraction curves at a local fiber volume fraction which correlates to the total fiber volume fraction at length scales above 14 µm. Local fiber volume fractions of 100% can only be observed at length scales below the fiber diameter, which is 7 µm here. Pure matrix areas contribute to local fiber volume fractions of 0% and can be observed to a length scale which is characteristic for the distribution. Notice that the periodicity in length scale is caused by superstructures in the artificial images due to the strictly periodic arrangement.

Subsequently, we apply the image processing method to artificial images showing fiber bundles of 7 and 19 fibers, respectively. Within the bundles the arrangement of the fibers is hexagonal and shows a fiber volume fraction of 82%. The bundles themselves are arranged in a cubic array. Altogether, the total fiber volume fraction is 42%. The artificial images and the respective results of the image processing method are shown in Figure 4 and Figure 5.

In the following, the results of the image showing bundles of 7 fibers (Figure 4) are discussed. They indicate a peak at 0% fiber volume fraction related to pure matrix regions between the fiber bundles. The area fraction gradually decreases up to a length scale of 18 µm, which correlates with the diameter of the circular gaps between the bundles. In addition, the bundles themselves are related to a peak in area fraction at approximately 80% local fiber volume fraction. At length scales up to 22 µm the maximum fiber volume fraction remains constant and then gradually declines to local fiber volume fractions of approximately 50% at 40 µm. The beginning of the decrease indicates the size of the bundles, which is 22 µm here. Furthermore, the area fraction drops after the peak at 32 µm length scale due to periodicity as observed in uniform fiber distributions. The substructures in the distributions correlate with smaller structures in the image. For instance, a local peak of 0% local fiber volume fractions shifts toward 35% at length scales up to 28 µm. This is related to small gaps of 7 µm diameter between the fiber bundles. The global peak center and the center of gravity of the distribution, respectively, indicate a total fiber volume fraction of 42%.

In Figure 5 the image processing method indicate similar results. The graph shows a two-peak structure at low length scale, as well. Pure matrix regions with 0% local fiber volume fraction contribute to the distribution up to a length scale of 35 µm. This is related to the maximum diameter of pure matrix areas. Moreover the maximum in local fiber volume fraction starts to shift at a length scale of 35 µm, which is correlated to the diameter of the fiber bundles. Again, substructures in the distributions are related to smaller features in the image. The center of gravity is equal to the total fiber volume fraction of 42%.

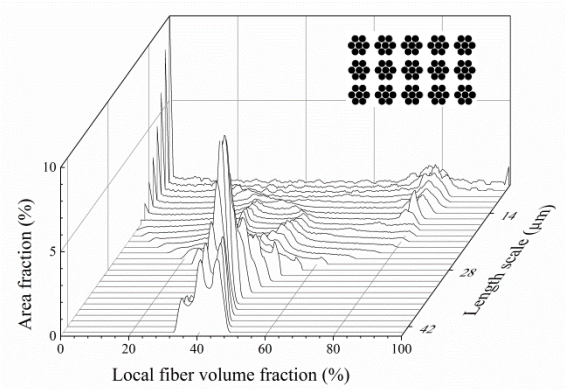

Figure 4. Area fraction of local fiber volume fractions in dependence of the observed length scale for simple non-uniform distributions with bundles of 7 fibers

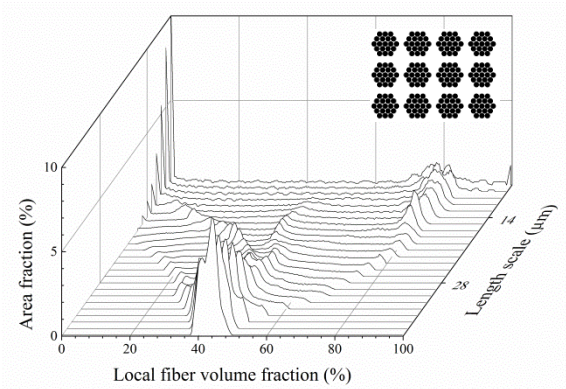

Figure 5. Area fraction of local fiber volume fractions in dependence of the observed length scale for simple non-uniform distributions with bundles of 19 fibers

3.2 Tapes

In the following, we apply the image processing method to the carbon fiber reinforced Polyamid-6 tapes T1 and T2 and discuss the results with respect to their micrographs. Therefore, we averaged the results of 30 images to cover a statistical sufficient area. We limited the maximum length scale to 50 µm due to the thickness of the tapes.

The results of the image processing method applied on tape T1 are shown in Figure 6. The area fraction shows two peaks on small length scales due to the two phase structure of the composite. The center of the first peak is at 0% local fiber volume fraction and is related to pure matrix regions. Its area fraction gradually decreases with increasing length scale and disappears at 18 µm which correlates to the maximum size of pure matrix regions in the micrographs, as shown in Figure 8. Furthermore, the second peak with approximately 80% local fiber volume fraction is related to fiber rich regions in the micrographs. Even at length scales up to 50 µm fiber rich regions contribute significantly to the area fractions. However, the two peaks merge at a length scale of approximately 28 µm. Accordingly, a distribution with one peak develops at large length scales. The center of the peak is at 55% local fiber volume fraction. With increasing length scale the center of gravity shifts towards higher values due to the reduced size of the region of interest, which is necessary due to the increased diameter of the mean filter. This indicates a higher fiber volume fraction in the center of the tape. In comparison, in Figure 7 the results of the image processing method for tape T2 indicate a double peak structure on small length scales, as well. Again, the first and second peaks are related to pure matrix regions and fiber rich regions, respectively. However, the maximum diameter of pure matrix regions is 50 µm here, which correlates with the diameter of pure matrix regions in the micrograph shown in Figure 9. Moreover, the two-peak structure remains at 50 µm length scale. This indicates a roving like structure, which can be observed in the micrograph, as well. Additionally, the center of gravity shifts towards higher values. Again, this indicates a higher fiber volume fraction in the center of the tape.

3.3 Laminates

The image processing method is applied to laminate P1 and P2 processed from tape T1 and T2, respectively. We limit the maximum length scale to 250 µm, which is approximately 1.5 times the tape thickness, because the micrographs do not indicate larger features in the samples.

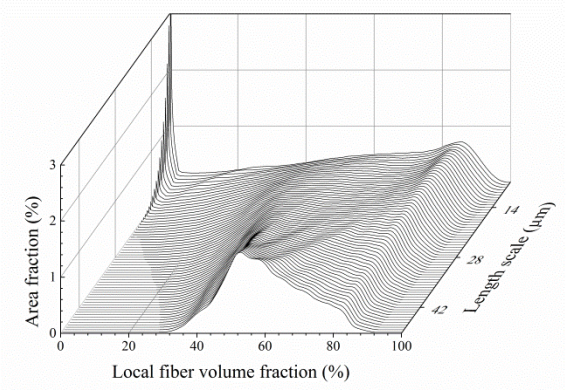

Figure 6. Area fraction of local fiber volume fractions in dependence of the observed length scales for tape T1

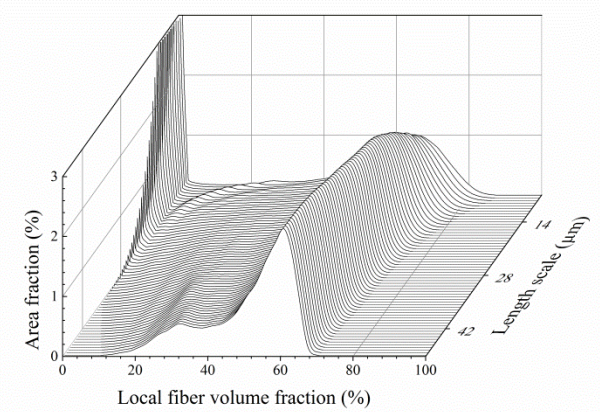

Figure 7. Area fraction of local fiber volume fractions in dependence of the observed length scales for tape T2

The area fraction of laminate P1 in Figure 10 indicates no significant deviation from a uniform fiber distribution even at length scales down to 38 µm. The results indicate the existence of pure matrix regions with a maximum diameter of 38 µm. The peak center as well as the center of gravity on all length scales is 43%. In contrast the results of laminate P2 in Figure 11 show a two-peak distribution in area fraction at length scales up to 120 µm. Again, the first peak is related to matrix rich regions and the second one to fiber rich regions. The peaks merge with increasing length scale and result in a single peak distribution. Here, the peak center and the center of gravity is 41%. Maximum diameter of pure matrix regions is evaluated to be 60 µm. A possible indicator for the homogeneity of the distribution is the width of the peaks on large length scale which is much smaller in laminate P1 compared to laminate P2.

Representative micrographs of laminate P1 and P2 show the characteristic features indicated by the image processing method. The micrograph in Figure 12 indicates the microstructure of laminate P1. It reveals a fiber distribution with local variations of fiber and matrix rich regions. However, on large length scales the distribution appears uniform. Pure matrix regions can only be observed up to a diameter of approximately 40 µm. On the contrary, fiber and matrix rich regions with diameters of approximately 120 µm are present in micrographs of laminate P2. Furthermore, pure matrix regions with diameter up to 60 µm are present in Figure 13. The roving structure in the laminate can clearly be identified and the fiber distribution is not nearly as uniform as in laminate P1.

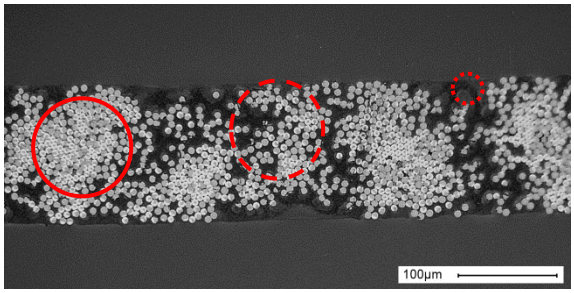

Figure 8. Micrograph of tape T1 with highlighted characteristic areas: local fiber volume fraction of 80% with radius larger than 50 µm (—), local fiber volume fraction of 40% with radius larger than 50 µm (– – –) and pure matrix region with radius of 22 µm (· · ·)

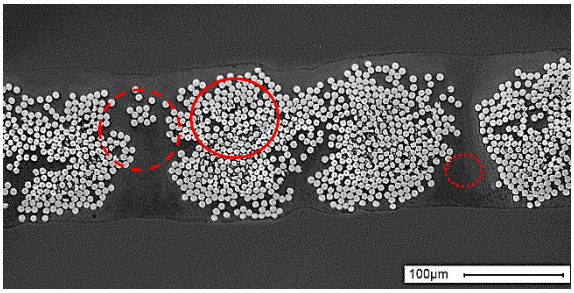

Figure 9. Micrograph of tape T2 with highlighted characteristic areas: local fiber volume fraction of 60% with radius larger than 50 µm (—), local fiber volume fraction of 25% with radius larger than 50 µm (– – –) and pure matrix regions with radius of 40 µm (· · ·)

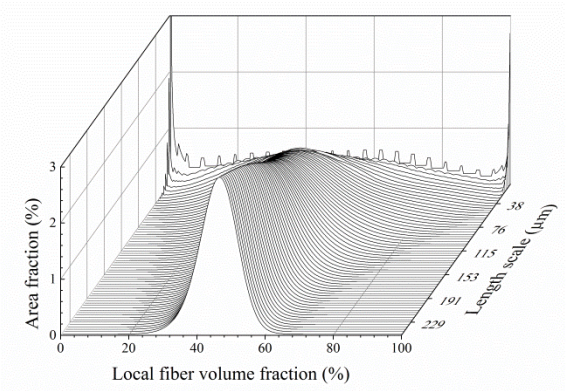

Figure 10. Area fraction of local fiber volume fractions in dependence of the observed length scales for P1

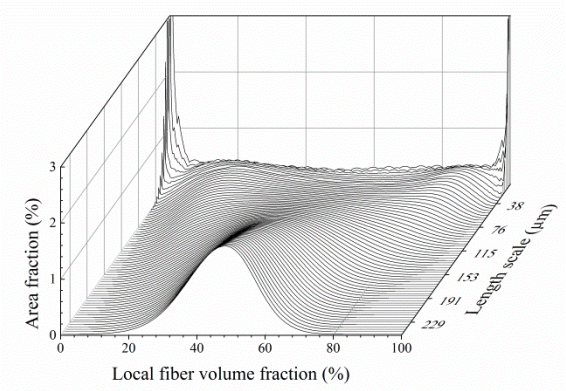

Figure 11. Area fraction of local fiber volume fractions in dependence of the observed length scales for P2

4. Conclusions

The image processing method is capable to quantify fiber distribution on different length scales. It reveals the microstructure of the composite in terms of local fiber volume fractions and provides an estimate of the length scale of the characteristic features, namely pure matrix regions and fiber bundles. Furthermore, roving like structures can be detected and quantified. Thus, the image processing method is a suitable tool to quantify the fiber distribution for process optimization of tape production and automated tape laying.

The results indicate a correlation between the fiber distribution of the tapes and their respective laminates. In summary, the double-peak distribution of tape T2 can still be observed in laminate P2 on small length scales. Although tape T1 shows a two-peak structure on small length scales, a single-peak distribution is observed in laminate P1 on every length scale. Therefore, we conclude that the tape laying and subsequent consolidation process is able to improve the fiber distribution on small length scales in the order of ten microns. However on larger length scales the non-uniform fiber bundle distribution remains in the produced laminates. Therefore, the tape laying process requires tapes with adequate homogeneity of fiber distribution to allow production of laminates of sufficient quality. It is worth noting that further data reduction is possible. For instance, an indicator of the homogeneity of a distribution can be defined using the standard deviation of the local fiber volume fraction on large length scales. Here, the distribution of laminate P1 yields a standard deviation of 15%, instead of 26% as in case of laminate P2.

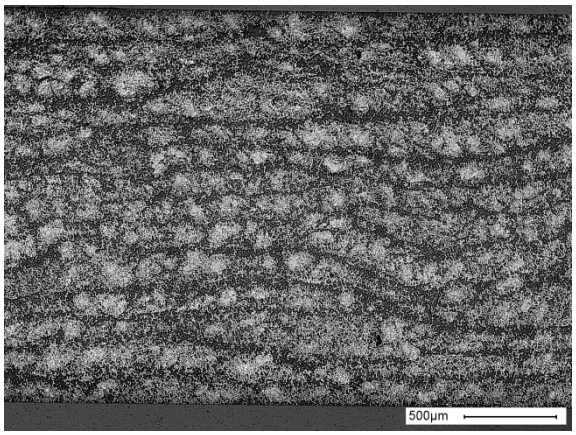

Figure 12. Micrograph of P1

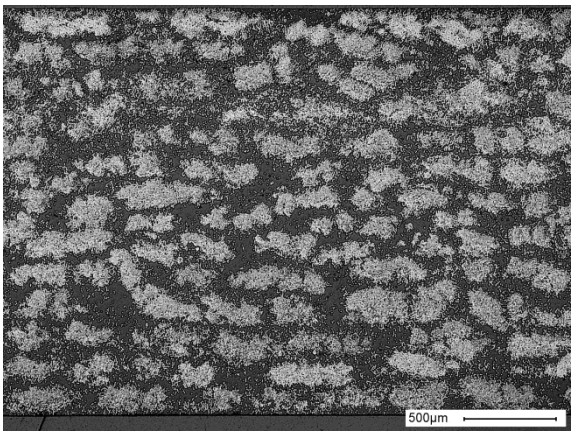

Figure 13. Micrograph of P2

An extension of the method to images of low contrast or resolution has to be evaluated. A customized scaling of the local fiber volume fraction axis with reference to the total fiber volume fractions obtained by the digestion method offers a method for investigating local fiber volume fraction without the need for single fiber detection. Especially for micro X-ray computer tomography this offers the evaluation of local fiber volume fractions, since the images are often not of sufficient quality to resolve single fibers.

References

[1] A. R. Maligno, N. A. Warrior, A. C. Long. Effects of inter-fiber spacing on damage evolution in unidirectional (UD) fibre-reinforced composites. *European Journal of Mechanics – A/Solids*, 28(4):768-776, 2009.

[2] M. Hojo, M. Mizuno, T. Hobbiebrunken, T. Adachi, M. Tanaka, S. K. Ha. Effect of fiber array irregularities on microscopic interfacial normal stress states of transversely loaded UD-CFRP from viewpoint of failure initiation. *Composites Science and Technology*, 69(11-12):1726-1734, 2009.

[3] V. Romanov, S. V. Lomov, Y. Swolfs, S. Orlava, L. Gorbatikh, I. Verpoest. Statistical analysis of real and simulated fibre arrangements in unidirectional composites. *Composite Science and Technology*, 87(0):126-134, 2013.

[4] T. Oktabe, M. Nishikawa, H. Toyoshima. A periodic unit-cell simulation of fiber-arrangement dependence on the transverse tensile failure in unidirectional carbon fiber reinforced composites. *International Journal of Solids and Structures*, 48(20):2948-2959, 2011.

[5] J.-L. Tsai, Y.-K. Chi. Investigating thermal residual stress effect on mechanical behaviors of fiber composites with different fiber array. *Composite Part B: Engineering*, 39(4):714-721. 2008.

[6] L. Ye, M. Lu, Y.-W. Mai. Thermal de-consolidation of thermoplastic matrix composites – I. Growth of voids. *Composite Science and Technology*, 62(16):2121-2130, 2002.

[7] L. Ye, Z.-R. Chen, M. Lu, M. Hou. De-consolidation and re-consolidation in CF/PPS thermoplastic matrix composites. *Composites Part A: Applied Science and Manufacturing*, 36(7):915-922, 2005.

[8] S. Ghosh, Z. Nowak, K. Lee. Quantitative characterization and modeling of composite microstructures by voronoi cells. *Acta Meterialia*, 45(6):2215-2234, 1997.

[9] J. Summerscales, F. J. Guild, N. R. L. Pearce, P. M. Russell. Voronoi cells, fractal dimensions and fibre composites. *Journal of microscopy*, 201(2):153-162, 2001.

[10] S. Gosh, Z. Nowak, K. Lee. Tessellation-based computational methods for the characterization and analysis of heterogeneous microstructures. *Composite Science and Technology*, 57(9-10), 1187-1210, 1997.

[11] R. Pyrz. Quantitative description of the microstructure of composites. Part I: Morphology of unidirectional composite systems. *Composites and Technology*, 50(2):197-208, 1994.

[12] A. Tewari ,A. M. Gokhale. Nearest neighbor distances between particles of finite size in three-dimensional uniform random microstructures. *Materials Science and Engineering: A*, 385(1-2), 332-341, 2004

[13] X. Chen, T. D. Papathanasiou. The transverse permeability of disordered fiber arrays: a statistical correlation in terms of the mean nearest interfiber spacing. *Transport in Porous Media*, 71(2):233-251:233-251, 2008.

[14] N. Otsu. Threshold selection method from gray-level histograms. *IEEE Transactions on systems man and cybernetics*, 9(1):62-66, 1979.